Available online at www.sciencedirect.com

ScienceDirect

Energy Procedia 92 (2016) 554 – 559

Energy Procedia

6th International Conference on Silicon Photovoltaics, SiliconPV 2016

Understanding the movement of cracked solar cell parts in PV-modules during mechanical loading

Felix Haase*, Jörg Käsewieter, Marc Köntges

Institute for Solar Energy Research Hamelin (ISFH), Am Ohrberg 1, 31860 Emmerthal, Germny

Abstract

We measure the three dimensional movement of cracked solar cell parts in standard sized PV-modules during a four line bending test. We develop a model which explains this movement assuming that the centers of mass of the solar cells or cell parts are fixed to the module glass. The widening of all cell gap widths is proportional to the bending roll displacement until a cell cracks in parallel to the bending rolls due to the tensile stress in the cells. At this point, the crack opens abruptly while the two parallel cell gaps next to the cracked cell close simultaneously by the same distance in sum. From here on, the cell gaps and the cell crack increases proportionally to the bending roll displacement. Since the distance between the centers of mass of both cracked cell parts is independent of the crack position, the crack width is also independent of the crack position for single cracks. Multiple parallel cracks in solar cells have smaller crack widths according to this model. Laminates without a backsheet show about 30 % larger crack widths.

Peer review by the scientific conference committee of SiliconPV 2016 under responsibility of PSE AG.

Keywords: Photovoltaic modules; Crack widths; Crystalline solar cells

1. Introduction

PV-modules sustain mechanical loads during their service lifetime [1,2]. If the PV modules are loaded mechanically from the front side, the whole layer stack of Ethylene-vinyl acetate (EVA), cells, and backsheet is under tensile stress [3]. Therefore the cells move apart from each other, since the EVA is much softer than the cells

* Corresponding author. Tel.: +49-5151-999-313; fax: +49-5151-5151-999-400.
E-mail address: felix.haase@isfh.de

Peer review by the scientific conference committee of SiliconPV 2016 under responsibility of PSE AG.
doi:10.1016/j.egypro.2016.07.019

in terms of the long-term Young's modulus [4]. At some point the stress in the cells exceeds the tensile strength and the cells crack. Cracked cell parts can significantly reduce the PV module power, if the size of the cracked cell part and the crack resistance at the crack exceeds a certain value [5-7]. Since the crack resistance depends on the crack width and its history [7], it is important to know about the movement of the cell parts in a PV-module.

In this contribution we measure the occurrence of cracks and the movement of the cell parts in standard sized frameless laminates in a 4 line bending setup. This introduces a homogeneous uniaxial stress field between the inner bending rolls, which allows for the same interpretation of the results for every cell in this area. We detect the stress induced cracks with electroluminescence (EL) [8] and measure the cell crack widths and cell gap widths by digital image correlation (DIC) [9].

2. Experimental

2.1. Sample preparation

We build three standard sized 60-cell laminates. Figure 1 shows the schematic cross section of the three laminates. All laminates are made from 60 commercial multicrystalline full-square three busbars solar cells each 15.6 × 15.6 cm^2 sized. An EL-transparent dot pattern is applied to the front side of the solar cells which allows measuring the movement of the cell parts by DIC and detection of the cracks by EL simultaneously. We place 10 solar cell strings each consisting of 6 cells in the laminate parallel to each other and to the short laminate edges (Fig. 2). The gap between the cells is d_{gw} = 4 mm in every direction. The size of the toughened safety glass laminate is 1680 × 1030 mm^2 with 3.2 mm thickness, the two sheets of EVA are each 460 µm thick. Laminate 1 has a 302 µm thick backsheet. Laminates 2 and 3 have no backsheets to evaluate the influence of the backsheet on the crack and gap widths. In Laminates 1 and 2 the cells are interconnected by standard cell interconnect ribbons, whereas Laminate 3 has no cell interconnect ribbons to investigate their influence on the crack and gap widths.

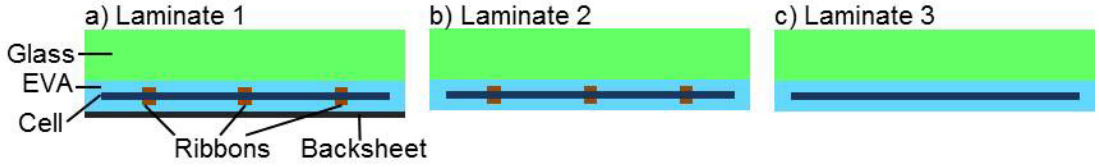

Fig. 1. Schematic cross section of Laminates 1-3 in (a) to (c). Laminate 1 is has a standard composition, Laminate 2 has no backsheet and laminate 3 has no backsheet and no cell interconnect ribbons.

2.2. Measurement setup

Figure 2a shows the setup for characterizing the PV laminate under mechanical load. The bending rolls of the 4-line bending setup have a distance of 1138 mm between their centers and are placed in front of the glass laminate whereas the bearing rolls have a distance of 1500 mm between their centers and are placed behind the laminate. We bend the laminate from a bending roll displacement d_{br} = 0 mm, where the laminate is flat, in steps of 5 mm to d_{br} = 95 mm. During the stops we take EL images of the center region of the laminate to investigate cell cracks [8]. Subsequent to the EL measurements the two cameras of the DIC use the pattern on the solar cells to calculate a three dimensional image [9]. The automatic evaluation software assumes straight rays reflected from the surface of the cells. In this case, the rays are optically refracted at the air / glass / EVA interfaces. Thus the real positions of the cells differ from the software calculations. We calculate these differences using the software evaluated positons of the cameras relatively to the glass surface and the incidence angle of the rays at the glass interface. Considering these differences we can calculate the real positions of the cells and thus the real gap and crack widths.

3. Results

Figure 2b schematically shows the part of Laminate 1 which we analyzed. From the three dimensional image of the cell surface we determine the change in the gap width Δd_{gw} and the crack width d_{cw} perpendicular to the bending rolls. In the center cell of the top row we detect a crack parallel to the ribbon in the EL image about 5 mm right of the left ribbon at d_{br} = 55 mm. The other five cells do not crack until d_{br} = 95 mm.

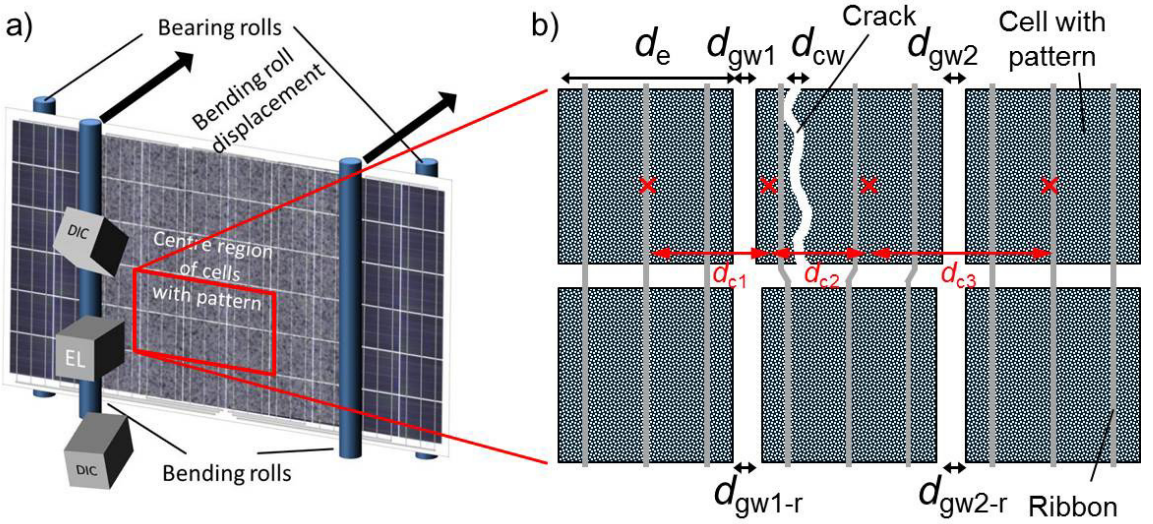

Fig. 2. a) Schematic drawing of the 4-line bending setup. The EL camera detects cell cracks and the DIC cameras measure the movement of the cell parts in the laminate. b) Schematic drawing of a part of the laminate. The cell interconnect ribbons are in parallel to the bending rolls. We evaluate the cell crack widths d_{cw} and cell gap widths d_{gw} from the DIC measurements perpendicular to the bending rolls. The red crosses are the centers of mass of the cell parts in the top row. The distances are marked by d_{c1}, d_{c2} and d_{c3}.

Figure 3a shows that the crack width d_{cw} remains 0 µm in the measurement uncertainty of 8 µm till d_{br} = 50 mm. At d_{br} = 55 mm the crack width increases abruptly until d_{cw} = 30 µm and increases proportionally to d_{br} up to d_{br} = 95 mm, indicated by the black line in Fig. 3a. The changes in the two gap widths increase proportionally to d_{br} with the same slope till d_{br} = 50 mm. At d_{br} = 55 mm Δd_{gw1} decreases abruptly and from here on increases proportionally to d_{br} till d_{br} = 95 mm. Δd_{gw2} shows the same characteristics, even though the abrupt decrease is much smaller and the slope is different. The sum S of all these distances increases proportionally to d_{br} from d_{br} = 0 mm to d_{br} = 95 mm.

Figure 3b shows the bottom row without any crack. Here, the changes in the two gap widths Δd_{gw-r} increase proportionally to the bending roll displacement d_{br} with a constant slope during the whole displacement. The sum of these two changes in gap width S_r has the same proportionality factor as the sum S of the top row.

4. Model of relative cell movement in laminate during bending

During mechanical loading of the laminate the neutral phase of the laminate is in the glass due to its thickness and its Young's modulus. Thus the rear side of the glass is under tensile strain which also strains the EVA. Since the EVA has a much lower long-term Young's modulus than the glass and the silicon, it deforms, that the silicon is strained much less. Thus the center of mass of the silicon does not move relatively to the glass and the gap between two cells opens. The four red crosses in Fig. 2b mark the centers of mass of the four cell parts in the top row after the crack.

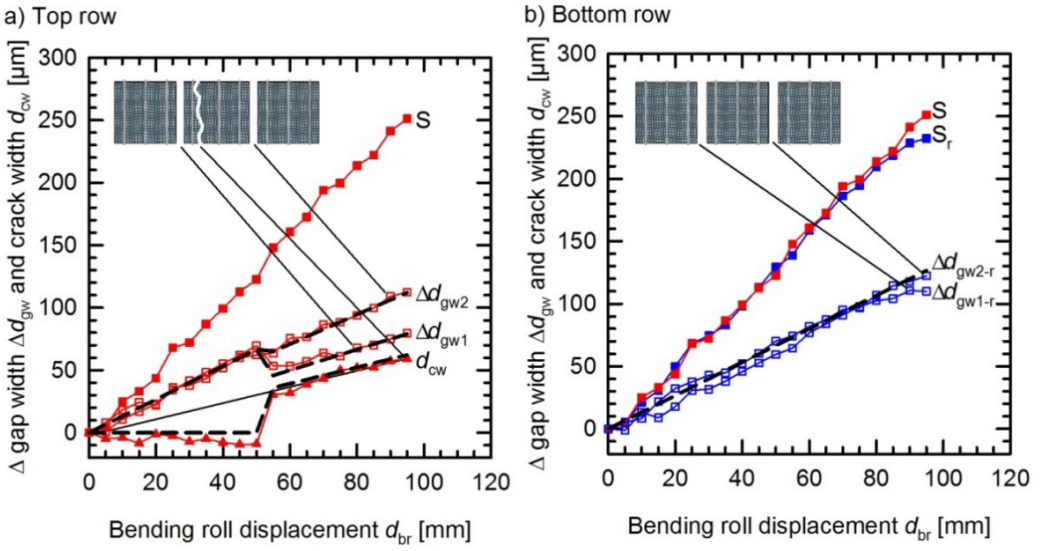

Fig. 3. a) shows the change in the gap widths (open squares), the crack width (triangles) and the sum of these (filled squares) of the top row in Fig. 2b. The dashed black lines show the values calculated with the model. b) shows the change in the gap width (blue open squares) and the sum of these (blue filled squares) of the bottom row of Fig. 2b. The dashed black lines show the values calculated with the model. For comparison we also plot the sum of the measured top row in red squares.

We suggest a model which assumes that during bending the centers of mass do not move relatively to the glass laminate and the cells are not strained, since we measure no strain of the edge length of the cells d_e in the measurement uncertainty of 8 µm. Thus, the distances of the centers of mass d_c in Fig. 2b increase proportionally to d_{br}. This results in following changes in gap widths

$$\Delta d_{gw1,2}(d_{br}) = S(d_{br}) \times d_{c1,3} \Big/ \left(\sum_{n=1}^{3} d_{cn} \right) \tag{1}$$

and crack width

$$d_{cw}(d_{br}) = S(d_{br}) \times d_{c2} \Big/ \left(\sum_{n=1}^{3} d_{cn} \right). \tag{2}$$

We evaluate the model by inserting the measured sum S of the top row into Eq. 1 and 2. We gain the crack and gap width, which are shown in Figure 3 by dashed black lines. Since the calculations are in agreement with the measurements within 12 µm in maximum, which is only slightly higher than the measurement uncertainty of 8 µm, our assumptions of the movements are confirmed. This is also confirmed in measurements for other single and multiple cracks.

This means that the cells drift apart from each other proportionally to the bending roll displacement until a crack appears. The cell cracks due to the tensile stress and the stress releases. Thus the cell parts drift away from each other abruptly and at the same time the parallel gaps close abruptly by the same distance in sum. The gap which is nearer to the crack is influenced more since the small cell part moves a wider distance than the big cell part.

With this model we can deduce for single cracks, that the crack width is independent of the crack position, since the distance of masses of the two cell parts d_{c2} equals always half of the cell edge length $d_e/2$ independently of the crack position in the solar cell. The model also explains, that multiple parallel cracks in solar cells have smaller crack widths since the sum is distributed to more cell cracks.

5. Influence of backsheet and cell interconnect ribbons on crack and gap width.

We can also use this model to compare the crack and gap width of laminates differing in the setup. We derive Eq. 1 and 2 by d_{br} and divide them by the distance of center of masses Δd_c and get Eq. 3 and 4, respectively:

$$\Delta d_{gw1,2} / \left(\Delta d_{br} \times d_{c1,3} \right) = \Delta S / \Delta d_{br} \Big/ \left(\sum_{n=1}^{3} d_{cn} \right). \tag{3}$$

and

$$\Delta d_{cw} / \left(\Delta d_{br} \times d_{c2} \right) = \Delta S / \Delta d_{br} \Big/ \left(\sum_{n=1}^{3} d_{cn} \right). \tag{4}$$

The right side of Eq. 3 and 4 contains no crack specific values and thus is constant in a laminate and characterizes the laminate specific correlation between bending and crack and gap opening.

We insert Eq. 3 in Eq. 4 and name the laminate specific crack and gap opening factor f_O:

$$f_O = \Delta d_{cw} / \left(\Delta d_{br} \times d_{c2} \right) = \Delta d_{gw1,2} / \left(\Delta d_{br} \times d_{c1,3} \right). \tag{5}$$

Thus we use all measured crack and gap widths with the corresponding distances of center of masses of a laminate to calculate the laminate specific crack and gap opening factor f_O for all three laminates in Fig 1. Every laminate is measured at 9 to 16 cracks or gaps. The resulting f_O-values of Eq. 5 are plotted in a box plot in Fig. 4.

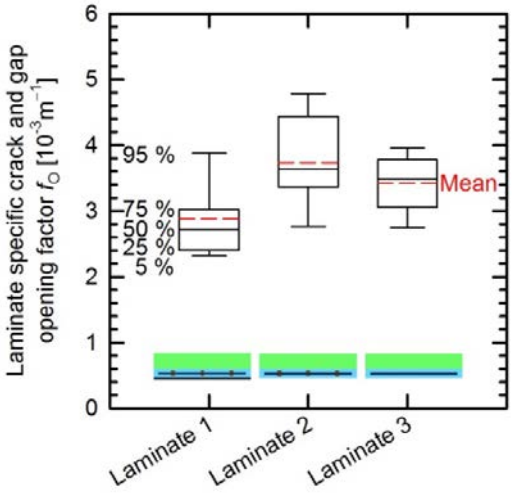

Fig. 4. Laminate specific crack and gap opening factor f_O for Laminates 1 through 3. The box plots mark the 5, 25, 50, 75 and 95 percentiles as well as the mean value.

Laminate 1 shows about 30 % lower values between the 25 and 75 percentiles than Laminates 2 to 3. Since Laminate 1 has a backsheet compared to the other two, the backsheet counteracts against the drifting apart of the cells and cell parts during bending. Laminate 2 has only slightly higher values than Laminate 3 which means that the cell interconnect ribbons in Laminate 2 have only a small contribution to the crack or gap widening during bending.

6. Conclusion

The absolute distances of cell movement are influenced by the exact setup of the laminates whereas the relative distances of cell movement can be described by a simple model introduced in this work, which assumes, that the center of mass of a cell is fixed to the glass of the laminate. From Eq. 5 we calculate the mean crack width for a single crack (d_{c2} = 78 mm) and a bending roll displacement at snow loads (d_{br} = 15 mm) [3] in the standard Laminate 1 to 3.4 µm. From [7] we know that big changes in crack widths can increase the crack resistance in less loading cycles. So crack widths should be kept small for the long term stability of a module. From this contribution we learn, that we should use a stiff backsheet, which counteracts against the drift apart from cell parts. Since the sum of crack widths is constant and if the crack resistance depends non-linearly on the crack width, it might be advantageous for minimizing the power loss in the module, to have single or multiple cracks in a cell depending on the crack position of the single or multiple cracks.

Acknowledgements

The authors would like to acknowledge Hilke Fischer and Iris Kunze for sample preparation and the Federal Ministry of Education and Research for funding this work in the Innovationsallianz: MIKRO 03SF0419A.

References

[1] M. Köntges, M. Siebert, A. D. Rodríguez, M. Denz, M. Wegner, R. Illing, and F. Wegert, “Impact of transportation on silicon wafer-based PV modules”, Proceedings of the 28th European Photovoltaic Solar Energy Conference, Paris, France, 2013, pp. 2960 - 2967.

[2] C. Olschok, M. Schmid, R. Haas, and G. Becker, “Inappropriate exposure to PV modules: description and effects of handling defaults”, Proceedings of the 28th European Photovoltaic Solar Energy Conference, Paris, France, 2013, pp. 3138 - 3141.

[3] F. Haase, J. Käsewieter, R. Winter, S. Blankemeyer, A. Morlier, I. Kunze, and M. Köntges, “Impact of backsheet on interconnector and cell breakage in PV laminates under mechanical loads”, Proceedings of the 29th European Photovoltaic Solar Energy Conference, Amsterdam, Netherlands, 2014, pp. 2477 - 2483.

[4] U. Eitner, M. Pander, S. Kajari-Schröder, M. Köntges, and H. Altenbach, “Thermomechanics of PV modules including the viscoelasticity of EVA”, Proceedings of the 26th European Photovoltaic Solar Energy Conference, Hamburg, Germany, 2011, pp. 3267 - 3269.

[5] M. Köntges, I. Kunze, S. Kajari-Schröder, X. Breitenmoser and B. Bjørneklett, “Quantifying the risk of power loss in PV modules due to micro cracks”, Proceedings of the 25th European Photovoltaic Solar Energy Conference, Valencia, Spain, 2010, pp. 3745-3752.

[6] A. Morlier, F. Haase, and M. Köntges, “Impact of Cracks in Multicrystalline Silicon Solar Cells on PV Module Power - A Simulation Study Based on Field Data”, IEEE Journal of Photovoltaics, vol.5, no.6, pp.1735-1741, Nov. 2015, DOI: 10.1109/JPHOTOV.2015.2471076.

[7] J. Käsewieter, F. Haase, and M. Köntges, “Model of cracked Solar Cell Metallization leading to permanent Module Power Loss”, IEEE Journal of Photovoltaics, vol.6, no.1, pp. 28-33, Jan. 2016, DOI: 10.1109/JPHOTOV.2015.2487829.

[8] U. Hoyer, C. Buerhop-Lutz, and U. Jahn, “Electroluminescence and infrared imaging for quality improvements of PV modules”, Proceedings of the 23rd European Photovoltaic Solar Energy Conference, Valencia, Spain, 2008, pp. 2913-2916.

[9] U. Eitner, M. Köntges, R. Brendel, “Measuring thermomechanical displacements of solar cells in laminates using digital image correlation”, Proceedings of the 34th IEEE Photovoltaic Specialists Conference, Philadelphia, 2009, pp. 1280–1284.